Cation effects on the hydrogen evolution reaction by catalysts based on cobalt complexes in alkaline electrolytes

Muhyuddin, M.; Pianta, N.; Trindell, J.A.; Ruffo, R.; Santoro, C.; Koper, M.T.M.

Electrochimica Acta 535 (2025) 146684

Contents lists available at ScienceDirect

Electrochimica Acta

journal homepage: www.journals.elsevier.com/electrochimica-acta

Cation Effects on the Hydrogen Evolution Reaction by Catalysts Based on Cobalt Complexes in Alkaline Electrolytes

Mohsin Muhyuddin [a], Nicolò Pianta [a], Jamie A Trindell [b], Riccardo Ruffo [a], Carlo Santoro [a], Marc TM Koper [b,*]

[a] Department of Materials Science, University of Milano-Bicocca, U5, Via Roberto Cozzi, 55, Milano 20125, Italy
[b] Leiden Institute of Chemistry, Leiden University, PO Box 9502, 2300 RA Leiden, The Netherlands

ARTICLE INFO

Keywords:
Hydrogen Evolution Reaction
Cobalt Phthalocyanine
Cobalt Porphyrin
Electrolytes Effects on HER
Cations Effects on HER
Role of pH
Alkaline Media
Concentration of Alkali Cations
Mass Transport

ABSTRACT

This study analyzes the influence of alkaline electrolytes on the hydrogen evolution reaction (HER) of the platinum group metal-free (PGM-free) electrocatalysts based on cobalt tetraphenylporphyrin (CoPor) and cobalt phthalocyanine (CoPc). The effect of pH (11-14), the nature and concentration of alkali metal cations (AMs^+), and the role of mass transport are elucidated. It is observed that HER catalyzed by both CoPor and CoPc is apparently a pH-dependent phenomenon where activity improves with an increase in the bulk electrolyte pH, while the overall cation trend is followed in the order of $K^+ > Na^+ > Li^+$. Li^+ cations support the HER up to pH 14, reaching a saturation level, particularly in the case of CoPor, whereas for CoPc activity continuously improves with the addition of Li^+. On the other hand, saturation is achieved at lower pH in the case of Na^+ and K^+ (at pH 13) with a clear HER inhibition at pH 14, i.e., HER activity decreases if the concentration of AMs^+ is further increased. Moreover, with the increase in the electrolyte mass transportation by increasing the rotation rate of the rotating disc electrode (RDE) deposited with either CoPor or CoPc, the corresponding HER activities tend to drop. We ascribe these trends to the interfacial cation concentration and how it is tuned by bulk cation concentration, pH, and mass transport. The estimation of the double-layer capacitance via electrochemical impedance spectroscopy (EIS) confirmed the enhanced concentration of AMs^+ at the reaction interface as the bulk pH or the concentration of the electrolyte increased.

1. Introduction

The hydrogen evolution reaction (HER) is one of the fundamental and most studied processes in electrochemistry. It has therefore remained the focus of scientific research, especially now that electrolysis-grade hydrogen is increasingly being recognized as a green energy vector. To realize the commercial integration of water electrolysis systems in the arena of the *Hydrogen Economy*, the prime reliance of HER on scarce and expensive platinum group metals (PGMs) must be curtailed. The transformation from an acidic medium to an alkaline electrolyte could play a key role in the given pursuit by allowing the use of abundant and cost-effective PGM-free transition metal (TM)-based electrocatalysts, which in these conditions are competitive compared to PGMs. However, the switch to an alkaline environment alters the activity descriptors and the reaction pathways (from proton reduction to water reduction), leading to additional bottlenecks, making the HER kinetically sluggish and significantly more complicated. The traditional activity descriptor for HER in acidic media, i.e., hydrogen binding energy (HBE) [1,2], fails to explain the non-Nernstian activity loss at higher pH on (single-crystal) platinum [3]. Instead, employing hydroxide adsorption as an HER activity descriptor in alkaline media highlights the importance of water as a proton donor and the necessity to break the O-H bond [4]. Moreover, water reorganization near the electrode interface in the alkaline media has also been suggested as an obstruction to charge transfer, ultimately impeding HER [5]. Typically, the inferior alkaline HER activity is mitigated through electrocatalyst design [6–9], but the role of electrolyte-electrode interaction is likewise critical to resolve [10].

Notably, slow HER in the alkaline media originates from the introduction of water dissociation as an additional energy barrier in the first electron transfer, i.e. the so-called 'Volmer step' [6,11–14] as the rate-determining step (RDS) [7]. As a result, the overall HER rate is affected by many factors, notably, the interaction of electrocatalytic surfaces with interfacial water molecules and their dissociation products

* Corresponding author,
E-mail address: m.koper@chem.leidenuniv.nl (M.T. Koper).

https://doi.org/10.1016/j.electacta.2025.146684
Received 27 January 2025; Received in revised form 5 June 2025; Accepted 7 June 2025
Available online 8 June 2025

in various electrochemical conditions. It has been observed that the presence of alkali metal cations (AMs^+) at a higher pH considerably influences the HER kinetics [15–18]. In an alkaline environment, interfacial AMs^+ may lower the activation barrier for water dissociation [19], presumably by favorably interacting with the transition state of the Volmer step by stabilizing the negative hydroxide ions being cleaved from the reacting H_2O molecule ($^*H–OH^{\delta-}– AMs^+$) [20,21]. However, the complete understanding of the interactions between AMs^+ and the electrocatalytic surface to launch HER is not yet fully disclosed. It may involve either direct non-covalent interactions or indirect electrostatic stabilization caused by AMs^+ at the cathode surface [19,21–24]. Under conditions of high local cation concentration, it also has the tendency to inhibit HER [20,24].

Xue et al. reported the opposing tendencies of AM^+ towards the capability of different metals to catalyze HER. Ir and Pt electrodes improve HER in the following order: LiOH>NaOH> KOH>RbOH>CsOH. On the other hand, the reverse trend is valid for Au and Ag [17]. It indicates that the AMs^+ have varying interactions and affinities towards different electrocatalytic surfaces. Weber et al. linked such effects on the kinetics of Pt with water arrangement regulated by non-covalent interactions of the hydrated cations and the adsorbed hydrogen, where the activation energy for the Volmer step would be lower for Li^+ than K^+ and Na^+[25]. In addition, the interaction of AMs^+ is also strongly dependent on the surface structure and oxophilicity of the electrocatalyst and AMs^+ interact distinctly with different morphologies and the oxophilic nature of the interface [5,26]. In addition to the identity of AMs^+, their concentration also influences the HER activity at a particular pH [16]. It was elucidated that AMs^+ tend to promote HER from low to mild alkalinity; however, in the higher pH regime, the increased near-surface concentration of weakly hydrated AMs^+ (K^+, Cs^+) inhibits the HER activity, while Li^+ promotes HER over the complete window of alkaline pH [24]. Recently, Ringe and Waegele et al. have reviewed the cation effects on HER activity, where we refer the reader to more detailed insights [15,27].

No doubt, the effect of AMs^+ on HER kinetics is important to decipher, making it a hotspot for contemporary research in electrocatalysis. Attention so far has been confined to PGMs and noble metals such as Au and Ag, whereas the ultimate goal of alkaline water electrolysis is to substitute PGMs with low-cost electrocatalysts. Single-atom electrocatalysts (SAEs) and molecular metal complexes in which first-row TMs exist in atomic-level coordination with nitrogen are emerging as candidates to replace PGMs [28–31]. In particular, cobalt stands out as a possible TM for this application [32,33]. Apart from a theoretical study on the influence of AMs^+ on the HER performance of the cobalt−dithiolene metal−organic frameworks (MOFs) [34], SAEs or molecular non-precious and PGM-free electrocatalysts have not yet received much attention experimentally. Recently, electrocatalysts based on cobalt phthalocyanine (CoPc) [35–38] and cobalt porphyrins (CoPors) [39–42] have shown encouraging activity for HER. Surendranath and coworkers attempted to uncover solvent-dependent concerted reaction mechanisms for CoPors attached to glassy carbon electrodes, where they can act like a metallic surface[43]. Likewise, CoPc and CoPor are also significant for other electrochemical reduction processes like the reduction of CO_2 [44,45], and O_2 [46–48].

This study systematically analyzes the electrochemical activity of alkaline electrolytes on the HER performance of PGM-free molecular electrocatalysts, focusing on CoPc- and CoPor-based electrocatalysts as model candidates. Specifically, we study HER activity in the alkaline pH window (11 to 14), as a function of the nature and concentration of AMs^+ present in the electrolyte. The role of mass transport on the HER activity under different electrolyte conditions was also thoroughly examined.

2. Materials and Methods

2.1. Materials

All the chemicals and reagents used in the study were of analytical grade with very high purity. They were used as is without further processing. The electrocatalysts used in the study, i.e, CoPor (5,10,15,20-Tetraphenyl-21H,23H-porphine cobalt(II)) and CoPc (Cobalt(II) phthalocyanine), were purchased from BDLpharm and Thermo Fisher Scientific, respectively. To prepare electrolytes, Alkali Metal Hydroxides (MOH) such as LiOH (99.995%) and KOH pellets (85+%) were purchased from Sigma-Aldrich, whereas Suprapur® 30% NaOH solution (Merck) was used. To analyze cation reaction orders, perchlorate salts $LiClO_4$ (99+ %, Thermo Scientific), $NaClO_4$ (99.99%, Sigma-Aldrich) and $KClO_4$ (99.99+%, Sigma-Aldrich) were used. All solutions were made using Ultrapure water (MilliQ gradient, ≥18.2 MΩcm, TOC < 5ppb). Before and during HER measurements, the electrolytes were purged with ultrapure Ar (6.0 purity, Linde) gas.

2.2. Electrode Preparation

To configure the working electrodes for HER measurements, CoPc and CoPor were deposited on the rotating disk electrode (RDE, Pine E5 Series with glassy carbon disk of 0.1963 cm^2 surface area). First, electrochemical ink was prepared according to previously published reports [49,50]. Briefly, 5 mg of CoPc or CoPor was dissolved in 985 µl of isopropanol and then 15 µl of Nafion® D-520 was added to the mixture. The vials containing the mixtures were sonicated using a probe sonicator for 30 minutes and subsequently transferred to the ultrasonic bath for 30 minutes to obtain a homogenous ink at room temperature. Next, the inks were carefully deposited via drop-casting on the RDE glassy carbon disk using a precision micropipette and left for drying under ambient conditions. The electrocatalyst loading on RDE was kept at 0.6 mg cm^{-2} for all the measurements. Importantly, for each measurement, every time, a fresh electrode was prepared by depositing a new loading. The structure of the electrocatalyst film was studied before and after HER using an Apreo S scanning electron microscope (SEM). The electrocatalyst-coated RDE discs were mounted on carbon tape and imaged directly. The micrographs were obtained using a T1 in-column detector in Optiplan mode with an accelerating voltage of 2.0 kV and a beam current between 50 and 200 pA.

2.3. Electrolytes

Fresh alkaline electrolytes with pH precisely varying from 11 to 14 were prepared using alkali metal hydroxides (MOH, where M =Li, Na, K). To study the cation reaction order in a particular MOH electrolyte with a defined pH, a pH-neutral perchlorate salt of the corresponding alkali metal was sequentially added. For MOH-based electrolytes, perchlorate salts ($MClO_4$, where M = Li, Na, K) were dissolved according to Table S1 at room temperature. The pH values of the achieved solutions were confirmed using a digital pH meter (XS pH80+DHS).

To exclusively analyze the pH-dependent and concentration-independent HER kinetics of CoPc and CoPor, different concentrations of NaOH electrolytes with specific pH values were brought to a constant ionic strength with respect to Na^+ cations by dissolving the respective concentrations of $NaClO_4$. The concentrations of Na^+ cations were kept at 1 M in the solutions with different pH values.

2.4. Electrochemical Measurements

All electrochemical experiments were carried out using a BioLogic multi-channel potentiostat/galvanostat (SP-300). A standard three-electrode system was used, comprising RDE as the working electrode, pure Au wire (0.5 mm diameter, MaTecK, 99.9%) as the counter electrode, and a reversible hydrogen electrode (RHE, Gaskatel, HydroFlex)

as a reference electrode. Moreover, considering the alkaline environment, a homemade Nalgene cell with PTFE seals was used and glassware was avoided in all experiments. A Pine RDE tip of the E5 series with PEEK shroud was utilized, which had a fixed glassy carbon disk with 0.1963 cm^2 surface area. To analyze the electrocatalytic activity under hydrodynamic situations, RDE was rotated at the desired RPM using a rotating assembly (Pine Research Instrumentation). The RDE disk was polished using a 0.25 μm polycrystalline diamond suspension (MetaDi, Buehler) and then cleaned by sonication in ethanol and ultrapure water (>18.2 MΩ cm, Millipore Milli-Q) for 10 minutes before the measurements (Bandelin SONOREX RK 52H). For each measurement, a fresh deposition of CoPc or CoPor was applied on the thoroughly cleaned glassy carbon disk of the RDE electrode.

To start with, cyclic voltammetry (CV) was performed to examine the HER activity of the configured RDE electrode with 0.6 mg cm^{-2} loading of CoPc or CoPor in the electrolyte of interest as described above. First, the electrocatalyst surface was conditioned by applying a few CV cycles at a 50 mV s^{-1} scan rate until a steady curve was obtained. Next, linear sweep voltammograms (LSVs) were acquired at a scan rate of 20 mV s^{-1}. The potential window was maintained between 0.07 to -1.0 V vs RHE. In all HER experiments, solution resistance was assessed through electrochemical impedance spectroscopy (EIS), and the electrode potential was automatically compensated for 85% of the ohmic drop. To analyze the operational durability of the samples, continuous CV over 500 cycles (at a 50 mV s^{-1} scan rate) was conducted in a deaerated 1 M NaOH solution. The initial and final LSVs were acquired at a scan rate of 20 mV s^{-1}, while the CV (at the scan rate of 20 mV s^{-1}) under stationary conditions prior and after the stability test were recorded in the potential window of -0.6 V to 1 V vs RHE.

EIS was performed using a similar three-electrode system at 1600 RPMs rotation rate. As before, freshly prepared CoPor electrodes were prepared by drop-casting 0.6 mg cm^{-2} loading on the cleaned RDE disk for each measurement. To acquire EIS data over various potentials, the staircase PEIS method was used in the range of 0.4 to -0.5 V vs RHE with 18 potential steps. For each step, the time to stabilize was kept at 30 sec. The frequency range was fixed between 200 kHz to 0.1 Hz with 6 points per decade. The sinusoidal amplitude was 25 mV, while an average of three measures per frequency was acquired. All impedances were fit using a homemade Python algorithm, mainly based on the "pymultipleis" library (GitHub link: https://github.com/richinex/pymultipleis), which exploits the "Adam" machine learning minimization method.

3. Results and Discussion

3.1. pH Effects

The investigation of the electrolyte effects on the HER activity of CoPor and CoPc began by elucidating the role of electrolyte pH in the alkaline window (11-14). Therefore, HER activity was first monitored with incrementing pHs in NaOH-based electrolytes while keeping Na^+ concentration fixed at 1 M. The observed trends are shown in Fig. 1 (a-d). It can be seen that, as the pH of the electrolyte increases from 11 to 14, the corresponding HER activity is boosted for both types of electrocatalysts. Moreover, the corresponding Tafel slopes of CoPor (Fig. 1c)

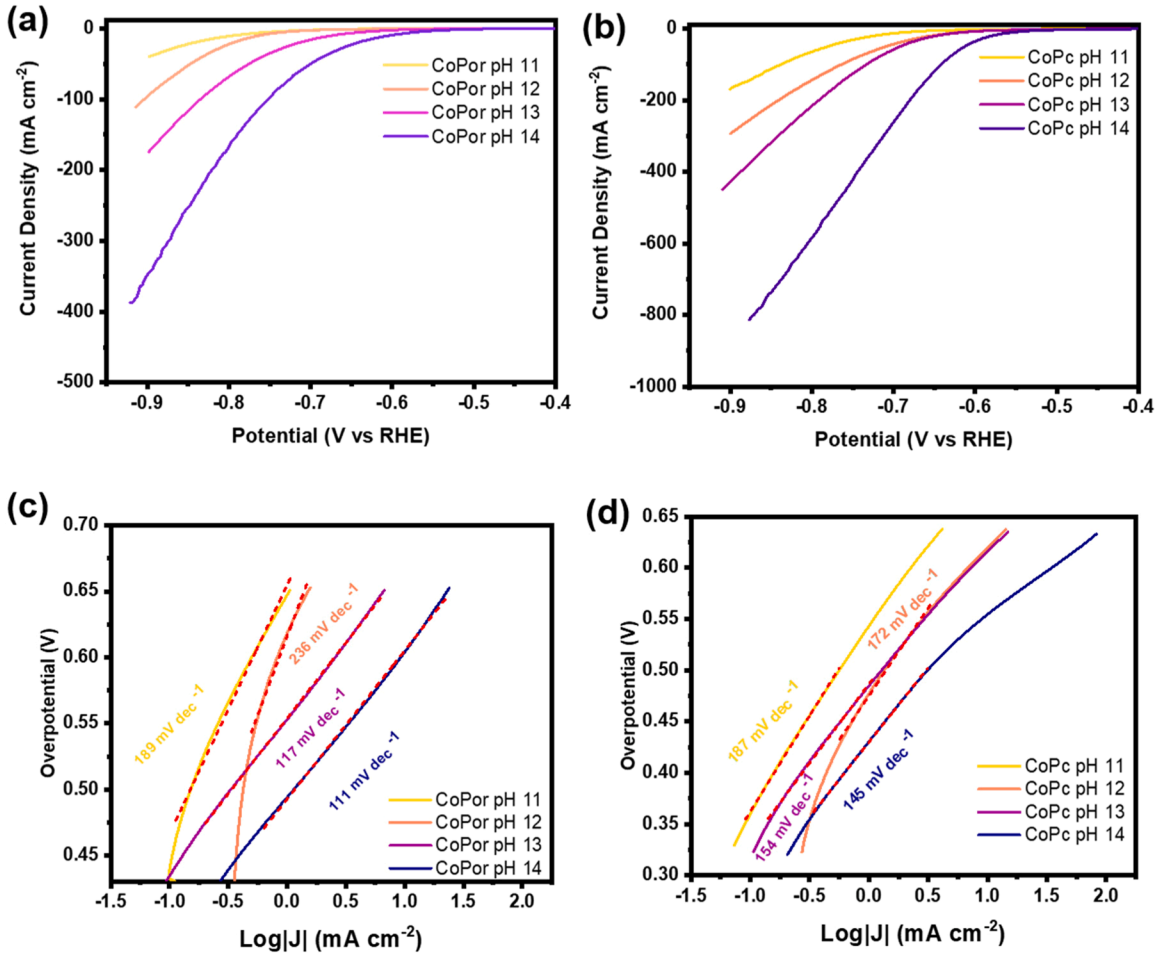

Fig. 1. HER activity under various conditions at 1600 RPM with a scan rate of 20 mV s^{-1}. HER polarization curves (a & b) and corresponding Tafel plots (c & d) for CoPor and CoPc under fixed Na^+ concentration of 1 M at different pH. At pH 11, the electrolyte contained 0.001 M NaOH plus 0.999 M $NaClO_4$, whereas 0.01 M NaOH plus 0.99 M $NaClO_4$ for pH 12, 0.1 M NaOH plus 0.9 M $NaClO_4$ for pH 13 and 1 M NaOH for the electrolyte having pH 14.

and CoPc (Fig. 1d) become smaller with increasing pH. The values of the Tafel slope, i.e. ~111 mV dec^{-1} for CoPor and ~145 mV dec^{-1} for CoPc at pH 14, indicate that the first electron transfer is rate limiting, i.e., the Volmer reaction is the RDS. The HER activities of CoPor and CoPc were also studied at different alkaline pHs in different MOH-based electrolytes i.e., LiOH, NaOH and KOH, with unfixed AMs$^+$ concentration (Fig. S1) and similar outcomes were observed with the activity increasing with increasing alkalinity. The HER polarization curves presented in Fig. 1 and S1 are additionally replotted with respect to the standard hydrogen electrode (SHE) by subtracting the factor of '0.0591 x pH' RHE from the potential values and the obtained trends are shown in Fig. S2 and S3, respectively. The SHE-scale data also demonstrate the enhancement in the HER kinetics with the increase in pH. It is important to underline that since the interfacial pH deviates from the bulk pH, especially at high current density and low bulk pH, all cation and pH trends are "apparent" trends with "apparent" reaction orders. This effect has been discussed at some length in refs [21,51,52], which can be referred to for further details

Previously, many recent studies have shown the pH-dependent nature of HER. Goyal et al. observed HER improvement on the gold surface with the increase in the pH at fixed AMs$^+$ concentration [53] and similar patterns for polycrystalline copper were noted by Resasco et al. [54]. Moreover, such pH-dependent HER activity of CoPor and CoPc agrees with the previous studies on different electrocatalytic surfaces [10,20, 21,24,55]. Traditionally, the enhancement in the HER kinetics has been explained with the help of the potential of zero charge (PZC) which positively shifts with respect to pH and hence under very high pH, a strongly negative electric field is developed at the interface that consequently increases the AMs$^+$ near-surface concentration to balance the increased negative charge density at the electrode's surface. Therefore, the enriched interfacial presence of AMs$^+$ contributes to the HER by stabilizing the transition state of the RDS, i.e., water dissociation during Volmer (*H–OH$^{\delta-}$– cat$^+$) [3,20]. It is important to mention that PZC measurements for molecular electrocatalysts are challenging, as these are highly heterogeneous in nature, involving multiple distinct active sites that differently take part in electrocatalysis. Another interesting aspect revealed during the study was the fact that the CoPc-based catalyst is relatively more active compared to the CoPor-based catalyst, as the current densities were higher at lower overpotentials. It might be due to different molecular structures and dissimilar ligand/-symmetric effects. However, the clarification of this aspect remains outside the scope of the presented study and requires an independent study.

3.2. Nature of the Cations

In an alkaline environment, HER is not only pH-dependent but also controlled by the nature of the AMs$^+$ present in the electrolyte. Therefore, it is rational to examine how different AM$^+$-containing electrolytes influence the HER kinetics of CoPor and CoPc. Fig. 2 shows a comparison of the overpotential values at different cathodic current densities i.e., -0.1 mA cm^{-2}, -10 mA cm^{-2} and -100 mA cm^{-2} for different 1 M MOH-based electrolytes at pH 14. For both CoPor and CoPc, the lowest activities were observed in the LiOH electrolyte, where the overpotentials were considerably higher compared to the other two types of electrolytes. KOH showed slightly higher activity than NaOH. It means that for CoPor and CoPc, AMs$^+$ promote HER in the order of $K^+ > Na^+ > Li^+$ which could be due to the relatively enhanced interaction of K^+ with the electrocatalyst surface. As discussed in the introduction, different metals demonstrate different affinities towards the AMs$^+$, hence the activity is altered accordingly. For PGM-free metals like Ag, Au and Cu, HER improves $K^+ > Na^+ > Li^+$, while Pt and Ir show an inverted trend. Therefore, the Co-based electrocatalysts used in the study exhibit similar trends with respect to AMs$^+$ identities when compared to PGM-free catalysts in previous studies [10,20,21,24,53,55].

3.3. Concentration Effects

The influence of AM$^+$ concentration was analyzed by sequentially adding pH-neutral perchlorate salt of the respective AM$^+$ at pH 11 to 14. The obtained LSVs are displayed in Figs. 3 and 4, while the corresponding reaction order plots are reported in Figs. S4 and S5. Interestingly, for both CoPor-based and CoPc-based catalysts, the HER activity has positive kinetic trends with respect to Li$^+$ concentration for all pH levels, as evidenced by the increase in current density. From the cation reaction orders, presented in panels (a-d) of Figs. S4 and S5, it can be observed that they tend to slightly decline when going from pH 11 to pH 13 but still remain positive, indicating improvement in the HER kinetics with a higher concentration of Li$^+$. As a notable observation, at pH 14, saturation is achieved in the case of CoPor and further addition of Li$^+$ does not contribute as significantly as it does at lower pH levels and the reaction orders eventually approach zero while for the CoPc addition of Li$^+$ still continuous to improve the activity. Instead, a different tendency was observed for the Na$^+$ and K$^+$-based electrolytes. At low pH 11 and pH 12 for both NaOH-based (panels a1-d1 of Fig. S4 and S54) and KOH-based (panels a2-d2 of Fig. S4 and S5) electrolytes, the respective AM$^+$ promotes the HER as indicated by the positive reaction orders. However, saturation was achieved at pH 13, whereas at pH 14, the reaction order became negative, indicating the inhibition of HER with higher AM$^+$ concentrations, predominantly in KOH-based media. On the contrary,

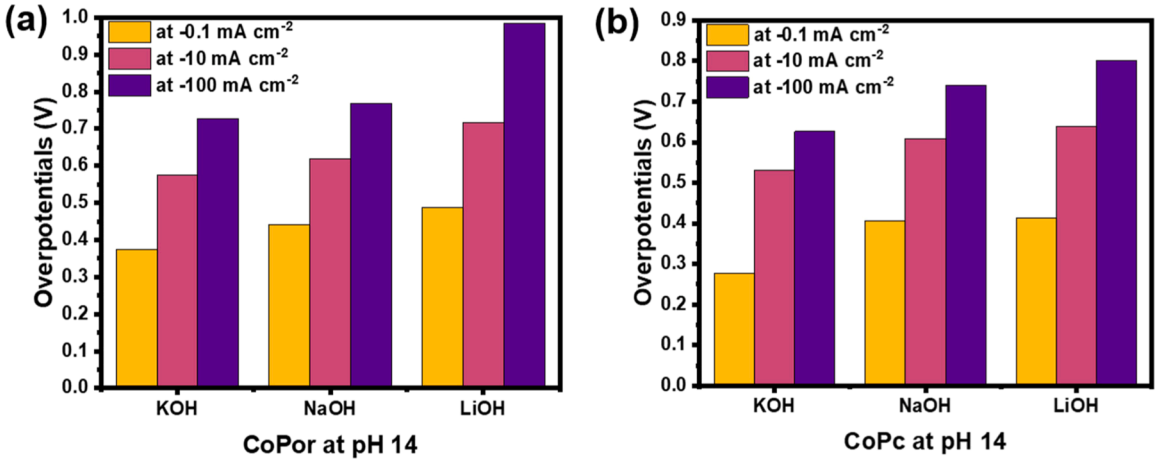

Fig. 2. Comparison of overpotential values at different current densities under varying 1 M MOH electrolytes at fixed pH 14.

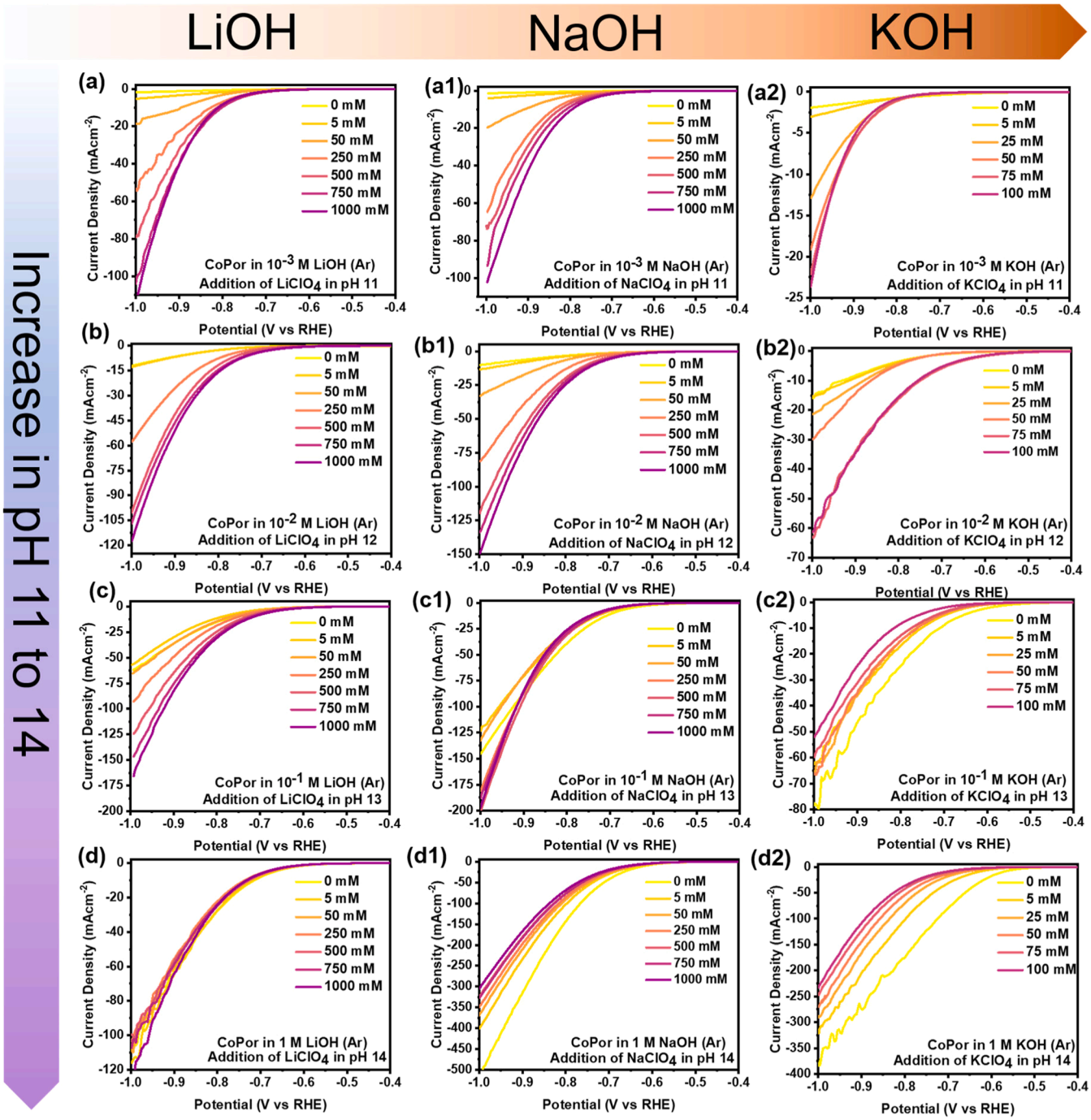

Fig. 3. HER polarization curves recorded on the 0.6 m cm^{-2} loading of CoPor on RDE rotating at a rotation of 1600 RPM in Ar-saturated MOH solutions. LSVs at the scan rate of 20 mV s^{-1} recorded in (a-d) LiOH-based electrolytes, (a1-d1) NaOH-based electrolytes and (a2-d2) KOH-based electrolytes. To analyze the effects of AMs^{+} concentrations, $LiClO_4$ and $NaClO_4$ were sequentially added up to 1000 mM concentrations in LiOH and NaOH-based solutions, respectively, whereas $KClO_4$ was added to a maximum concentration of 100 mM due to its solubility limit.

for CoPc, HER order reactions remained in the saturation phase at pH 13, but at pH 14, HER inhibition occurred. In fact, a careful look at the KOH-based electrolyte with pH 14 (Fig. S5 (d2)) indicates an initial restoration in the cation order reaction, which eventually becomes very negative at higher concentrations, as can also be seen in the corresponding LSVs provided in Fig. 4 (i). The pH dependence of HER reaction orders with respect to cation concentration indicates a correlation between the electrolyte pH and the near-surface cation concentration. Monteiro et al. has observed similar cation order trends for Au and Pt electrocatalysts, with Li^{+} always promoting HER while bigger cations i. e. K^{+} and Cs^{+} show promotion, saturation and then inhibition with increasing pH [24]. The inhibition of HER at high interfacial cation concentration is typically attributed to the AM^{+} chemisorbed in the inner Helmholtz plane [20,56]. Apparently, after a certain threshold, near-surface AM^{+} accumulation could have detrimental effects on HER if the AM^{+}–electrocatalyst interactions are enhanced at the expense of water– electrocatalyst interactions [21]. Moreover, Tanaka and co-workers observed that heavier AM^{+}, i.e., Cs^{+} attracted closer to the Pt surface to build a bilayer structure in CsOH that prevents the adsorption of water molecules on the Pt surface and causes the inhibition of HER [57]. Despite this, it is essential to recognize that Li^{+} ions are fully hydrated, with tightly bound water molecules in their hydration shell,

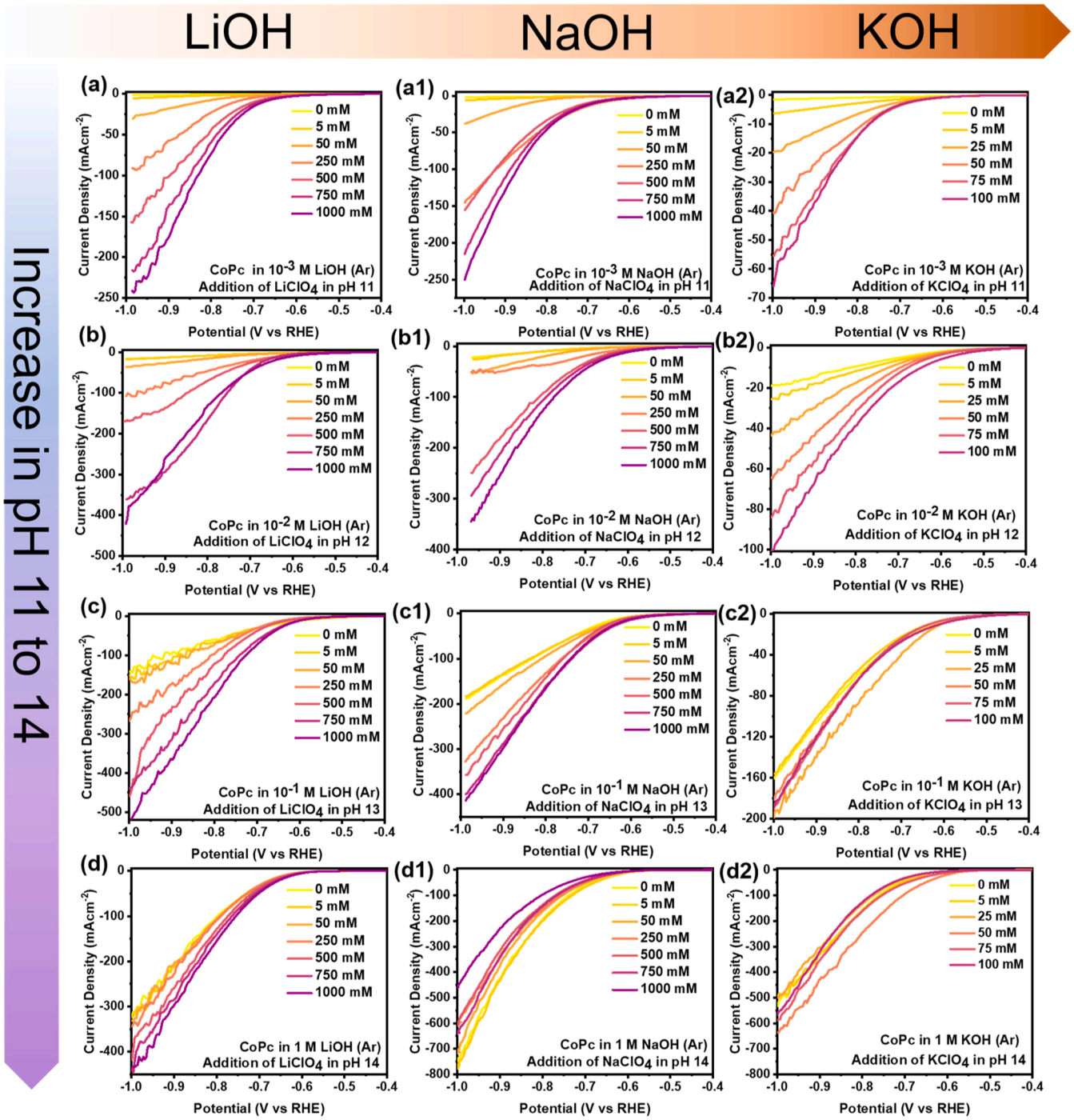

Fig. 4. HER polarization curves recorded on the 0.6 m cm^{-2} loading of CoPc on RDE rotating at rotation of 1600 RPM in Ar-saturated MOH solutions LSVs at the scan rate of 20 mV s^{-1} recorded in (a-d) LiOH-based electrolytes, (a1-d1) NaOH-based electrolytes and (a2-d2) KOH-based electrolytes. To analyze the effects of AMs^{+} concentrations, $LiClO_4$ and NaClO4 were sequentially added up to 1000 mM concentrations in LiOH and NaOH-based solutions respectively, whereas the $KClO_4$ was added to a maximum concentration of 100 mM due to its solubility limit.

which would prevent them from overcrowding near the outer Helmholtz plane and inhibiting the HER. On the other hand, weakly hydrated cations like Na^{+} and K^{+} have partially dissolved solvation shells, tend to accumulate near the electrode, and initially enhance HER by stabilizing water dissociation; however, above a certain threshold concentration, they apparently block active sites and inhibit HER [19,24,58,59].

3.4. Mass Transport

Next, the role of mass transport using RDE under different MOH alkaline electrolytes (pH 11- 14) was analyzed as shown in Figs. 5 and S6, for CoPor and CoPc, respectively. It can be seen that as the rotation rate of RDE increases from 0 to 2500 RPMs, the HER activities tend to decline. This overall trend is observed irrespective of pH and the nature of the electrolyte. However, at very high overpotentials, bubble formation affects the current densities under stationary conditions and low rotation rates of the RDE. This effect was more prominent at higher pH conditions, i.e. 13 and 14, due to the correspondingly enhanced HER activity. In fact, at higher overpotentials, excessive hydrogen bubble formation can reduce the current densities by shielding the

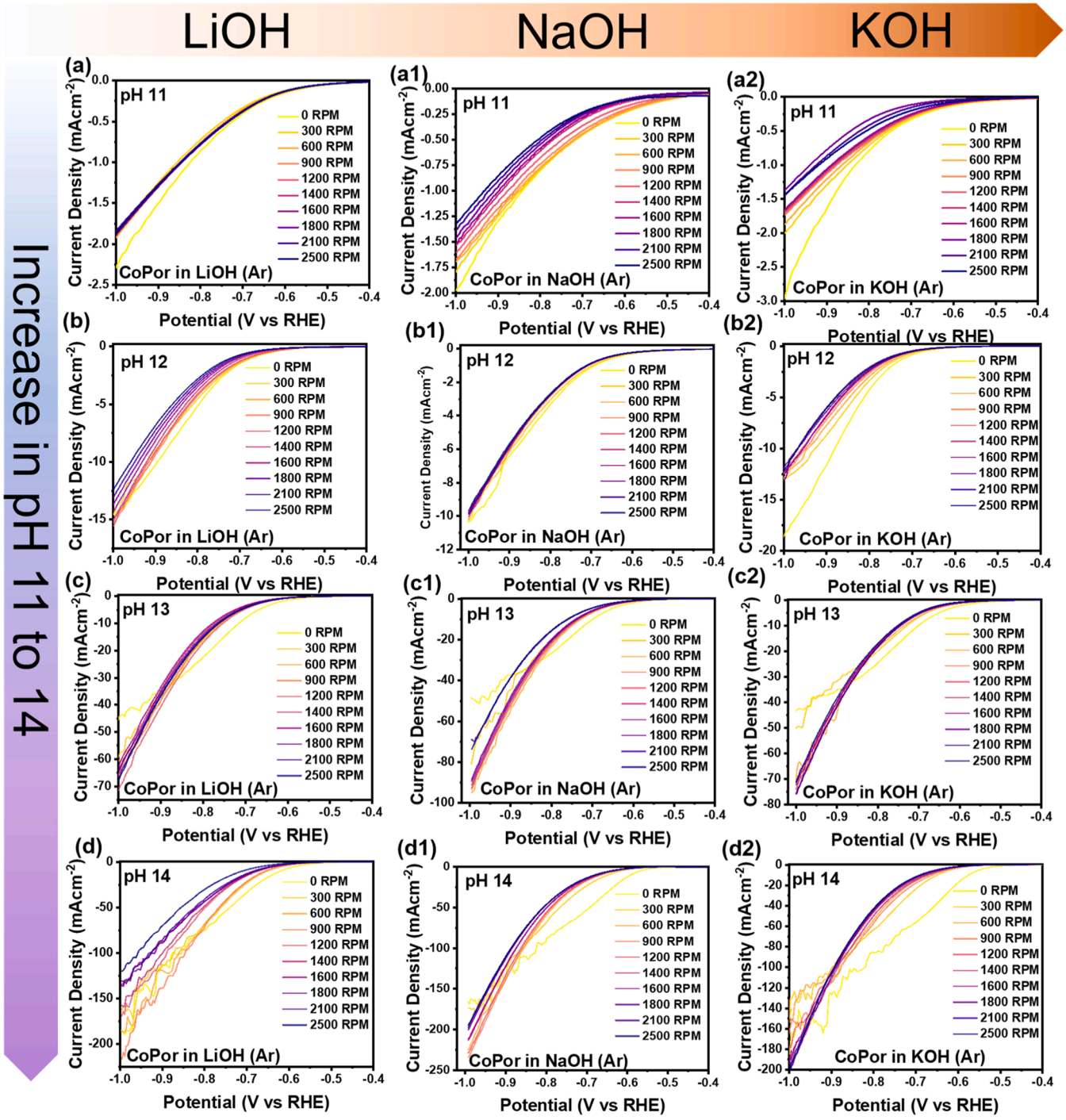

Fig. 5. HER polarization curves recorded on the 0.6 m cm^{-2} loading of CoPor on RDE rotating at different rotations (0, 300, 600, 900, 1200, 1400, 1600, 1800, 2100, 2500 RPM) in Ar-saturated MOH solutions. LSVs at the scan rate of 20 mV s^{-1} acquired in (a-d) LiOH-based electrolytes, (a1-d1) NaOH-based electrolytes and a2-d2) KOH-based electrolytes. The pH increases from top to bottom. Panels (a, a1 & a2) correspond to pH 11, (b, b1, & b2) correspond to pH 12, (c, c1, & c2) correspond to pH 13 and HER trends under pH 14 are displayed in the panels (d, d1, & d2).

electrocatalyst's active surface area [60]. By increasing the RDE rotation, this issue can be overcome by promoting the disengagement of evolving bubbles. In any case, the negative impact of enhanced mass transport on HER activities is very evident, particularly between 0 and ca. -0.8 V vs RHE. Theoretically, HER in alkaline media should remain unaffected by mass transport constraints and diffusion limitations due to the high concentration of water as a reactant. Recently, the contrasting role of mass transport in tuning the HER kinetics, showing trends similar to those observed for CoPc and CoPor, was reported on Au electrodes, where activity decreased with increasing rotation speed [21]. The reason for the activity reduction can be ascribed to the increase in the concentration of the locally generated hydroxyl ions in the vicinity of the electrode interface. The effect of mass transport is then on transporting these hydroxyls away from the interface, such that the local pH increase is less for a higher rotation rate. This local pH increase also leads to a corresponding increase in the near-surface AM^{+} concentration to maintain the local electro-neutrality. In turn, the HER activity is affected because these AM^{+} are essential for stabilizing the water

dissociation during the rate-limiting Volmer step, as already discussed [21,53]. Liu et al. have verified the variation of the interfacial pH with respect to the electrode's rotation rates [52]. Therefore, the modification in the local alkalinity and correspondingly the AM^{+} gradient is more likely to be the reason for HER performance decay with higher rotation rates.

3.5. Structural stability

The structural integrity of the CoPc and CoPor-based electrocatalyst films on RDE before and after performing HER was analyzed using SEM. From the micrographs reported in Fig. S7, the structure of the CoPc-based electrocatalyst was significantly changed after the HER experiments. Specifically, after the HER, Co nanoparticles were observed throughout the exposed surface, indicating limited structural stability. In contrast, the CoPor-based electrocatalyst seemed to form a more dense film on the electrode surface. Overall, it appeared that these CoPor films were relatively stable during HER, with no obvious structural changes or nanoparticle formation observed via SEM (Fig. S8). To validate the operational durability, an accelerated stability test over the 500 CV cycles in 1 M NaOH was conducted for both electrocatalysts and the outcomes are demonstrated in Fig. S9. Over the 500 CV cycles, CoPor displays a negligible difference in HER polarization, while CoPc exhibits a significant alteration in HER kinetics along with noticeable suppression of redox peaks in the full scan CV (inset of Fig. S9 (b)). In fact, after continuous cycling, the HER overpotential of CoPc was considerably reduced, which could be attributed to the evolution of the nanoparticles since improvement in the HER due to the transformation of metal phthalocyanine structures into nanoparticles has already been reported [31]. It should be noted that the structural durability and modes of electrochemical degradation are independent and complicated research topics that require separate in-depth investigations. While falling

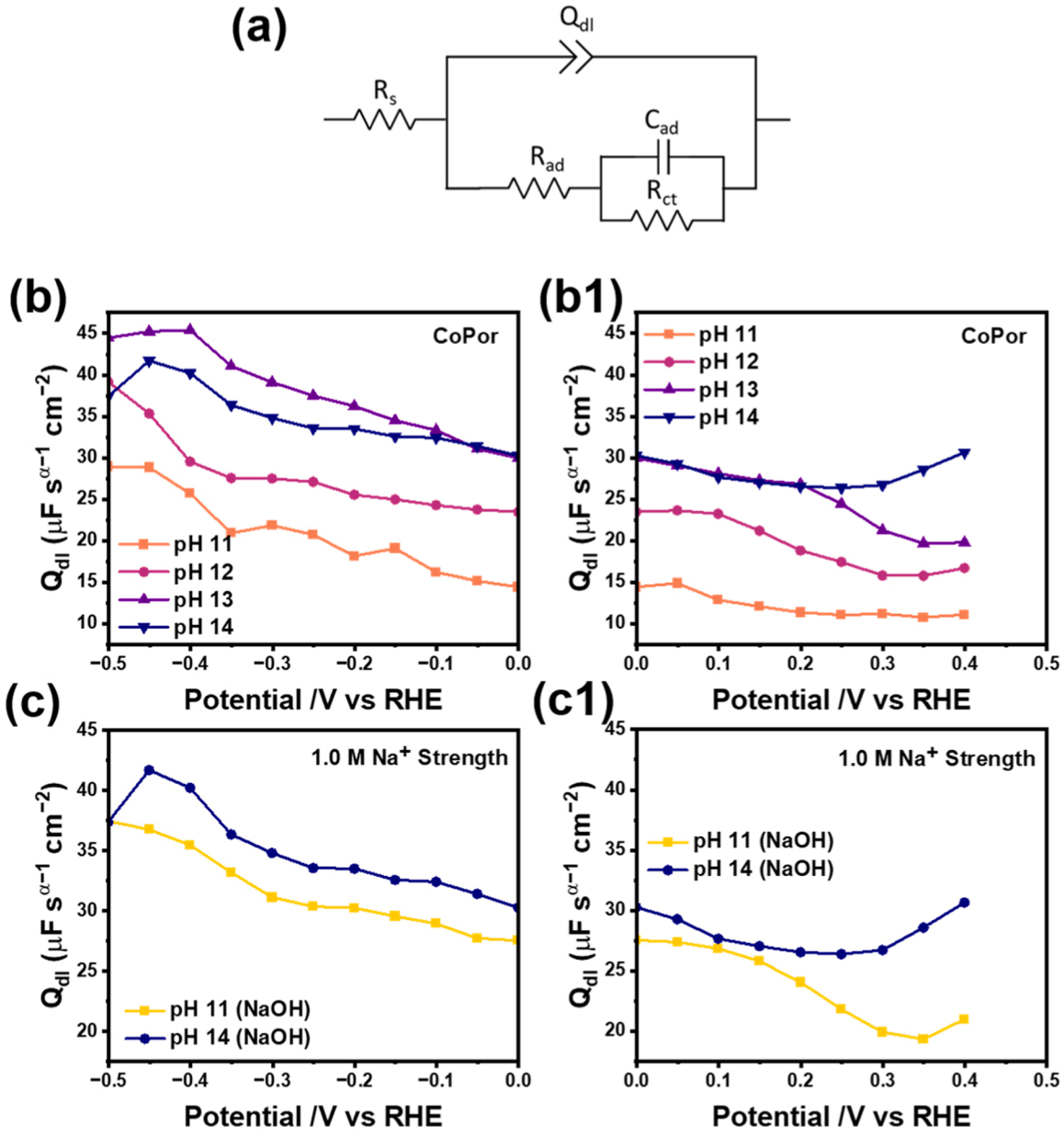

Fig. 6. EIS results of CoPor-based electrocatalyst in the double layer region and HER potential window as a function of pH in NaOH electrolytes. (a) The equivalent circuit representing a Volmer-Heyrovsky HER route used for fitting the EIS data. Constant phase "double-layer capacitance" (Q_{dl}) as a function of pH with different Na^+ concentrations (b & b1) and pure pH response with the same 1.0 M Na^+ strength (c & c1) calculated in both faradaic (b &c) and non-faradaic potential regions (b1 &c1).

outside the scope of the presented work, it provides an opportunity for future research to be considered. Therefore, the interfacial analysis was performed on the CoPor-based electrode, showing slightly better stability during the measurements.

3.6. Interfacial analysis

As discussed above, both pH and AM^+ concentration have an impact on the HER kinetics. HER performance generally improves with pH; however, after a certain level, presumably related to a critical local cation concentration, saturation is reached and subsequently, an inhibitory effect of AM^+ is observed (i.e. pH 14) [19,21]. Yet it remains uncertain whether the AMs^+ chemisorb on the electrocatalytic sites or merely accumulates in the double layer, leaving the exact cause of HER inhibition not fully understood [20]. In the absence of any direct characterization methodology for the precise estimation of the AM^+ concentration at the interface, measuring the interfacial capacitances (double-layer capacitance) could be the first way to examine the potential variations in interfacial AM^+ concentration [18,20], and to correlate with HER activity. Fig. 6 shows the results of the key interfacial events during the HER by CoPor as a function of pH. The equivalent circuit used to fit the acquired Nyquist plots (typical examples provided in Fig. S10) is presented in Fig. 6a. Bandarenka et al. previously used this circuit to analyze the Volmer-Heyrovsky HER pathway [61,62]. In principle, the proposed model is mainly expected to fit the data in the faradaic region, while failing elsewhere. Interestingly, a small background current was observed even at positive potentials, probably due to the manifestation of a side reaction. Therefore, we decided to fit the whole dataset with the aforementioned model, while maintaining a more conventional nomenclature for the potential regions (i.e., "double-layer" region for positive potentials and "HER" region for potentials from zero downwards). The circuit can be divided into the following parts: (i) series resistance (R_s) mainly related to the ohmic resistance of the electrolyte, (ii) the non-Faradaic capacitative branch modeled by a so-called constant phase element (Q_{dl}) and (iii) the Faradaic branch representing HER comprised of a charge transfer resistance (R_{ct}), adsorption resistance (R_{ad}), and adsorption capacitance (C_{ad}). If the double-layer capacitance follows the Gouy-Chapman model [63], it should scale with the square root of the interfacial cation concentration. Although the conditions with the Gouy-Chapman model are not quantitatively met (i.e. high concentration, very negative potential with respect to PZC), we consider that the interfacial capacitance may still be a (rough) measure for local cation concentration, as assumed previously [17,20,23,26,58].

The frequency dependence of the capacitive constant phase element, Z_{CPE}, is modeled using:

$$Z_{CPE} = \frac{1}{(j\omega)^{\alpha} Q_{dl}} \quad (1)$$

which gives the CPE double layer "capacitance" Q_{dl} and the CPE exponent α. If the parameter α is above 0.95, Q_{dl} is a good representation of C_{dl}.

From Fig. 6(b & b1) it can be seen that as the pH of the electrolyte increases the Q_{dl} in the double layer (0.5 to 0.0) and near HER (0 to -0.5) regions increases until pH 13. The Q_{dl} values appear to be higher at pH 14 compared to those at pH 13 in the double-layer region, and then slightly drop when approaching the HER region (Fig. 6b). In any case, the increase in the Q_{dl} with increments in the pH suggests a relative increase in the concentration of interfacial AMs^+. However, the slightly lower Q_{dl} values in pH 14 (near HER region) compared to pH 13 agree with the transition to a negative reaction order observed under these conditions (see the transition from promotion to inhibition in Fig. 3c1 to Fig. 3d1). This strongly suggests that the local AMs^+ concentration near the interface plays an important role in the HER kinetics. To further validate this argument, the pure pH response on the HER kinetics of CoPor irrespective of the AMs^+ concentration was analyzed by additionally performing EIS at pH 11 with Na^+ strength equal to that of pH 14 (1.0 M) by adding 0.999 M of $NaClO_4$ and the outcomes are reported in the supplementary information as Fig. 6 (c &c1). The EIS results further confirmed the influence of pure pH on the HER kinetics of the CoPor-based electrocatalyst. When the cationic strength of the solution remained at 1.0 M, Q_{dl} systematically increased with an increase in the pH from 11 to 14, confirming again the enhanced AMs^+ interfacial concentration. The observation supports that the HER improvements as a function of electrolyte pH are likely related to changes in interfacial cation concentration.

To gain more insights into the effect of AMs^+ concentration, EIS was also run under pure electrolytic (NaOH) conditions and with the addition of 250 mM $NaClO_4$ in alkaline pH 11 & 12. Notably, Q_{dl} increased in the same way when the concentration of Na^+ was raised by adding the aforementioned quantity of $NaClO_4$ in both pH levels (Fig. 7). Here, the takeaway is that both electrolyte pH and bulk AMs^+ concentration have a similar impact on the electrode-electrolyte interface. The same interfacial characteristics were analyzed under different pure MOH (M = Li, Na, K) electrolytes at pH 14 as provided in Fig. S12. Interestingly, Q_{dl} in the case of KOH electrolyte was significantly higher compared to that of NaOH and LiOH, indicating enhanced interaction of K^+ with the CoPor-based RDE. Bandarenka's group also observed for various electrode surfaces that the capacitance scales with the hydration energy of AM^+, following this order: $Li^+ < Na^+ < K^+ < Rb^+ < Cs^+$ [18,58]. It is noteworthy to recall that the same trend for the HER activity has already been confirmed for CoPor, where the peak performance was achieved with KOH-based electrolytes.

4. Perspective

In this work, the effect of the electrolyte, particularly in the alkaline range, towards HER on CoPc and CoPor-based electrocatalyst films on RDE was comprehensively investigated. The role of mass transport, varying pH, identity and concentration of the AMs^+ along with interfacial attributes were detailedly analyzed. As an effort to elucidate the electrolytic effects on the HER activity of PGM-free transition metals-based electrocatalysts, our discussion frequently referenced (single-crystal) metal electrodes such as Pt or Au. However, from the materials science perspective, comparing the performance metrics of the molecular electrocatalysts with those of single-crystal pure metallic surfaces raises several questions. It should be emphasized that molecular electrocatalysts comprise a multitude of active sites, each uniquely contributing to the electrochemical activity, with the overall response being the collective effect of all these sites or moieties. Moreover, in addition to the metallic centers with nitrogen coordination, the surrounding organic ligands and non-metallic sites could also be redox-active and participate in the reaction. The electrocatalytic degradation of such electrocatalysts is also an important consideration, particularly in their pure molecular nature. Here, surface chemistry and molecular coordination become inevitably important. Since their structures are very heterogeneous and morphological parameters could also vary, the electrolytic response should also be analyzed while considering material properties. During the electrochemical activity, the active sites may also undergo important transformations (e.g. aggregation, losing the metallic center, changing configuration, etc) and/or poisoning. It is crucial to specify which active sites experienced promotion, saturation, and inhibition levels during the HER process, as well as the methods used to identify these changes. Furthermore, the mechanisms of such electrochemical phenomena have to be determined. Synchrotron measurements to actually analyze the interaction of electrolyte components with the electrocatalyst under operando conditions may experimentally validate the various hypotheses regarding the electrolyte effect. Post-mortem examination of the electrocatalysts under varying electrolytic conditions should also be pursued and compared with the initial pristine HER conditions. By combining the experimental outcomes with

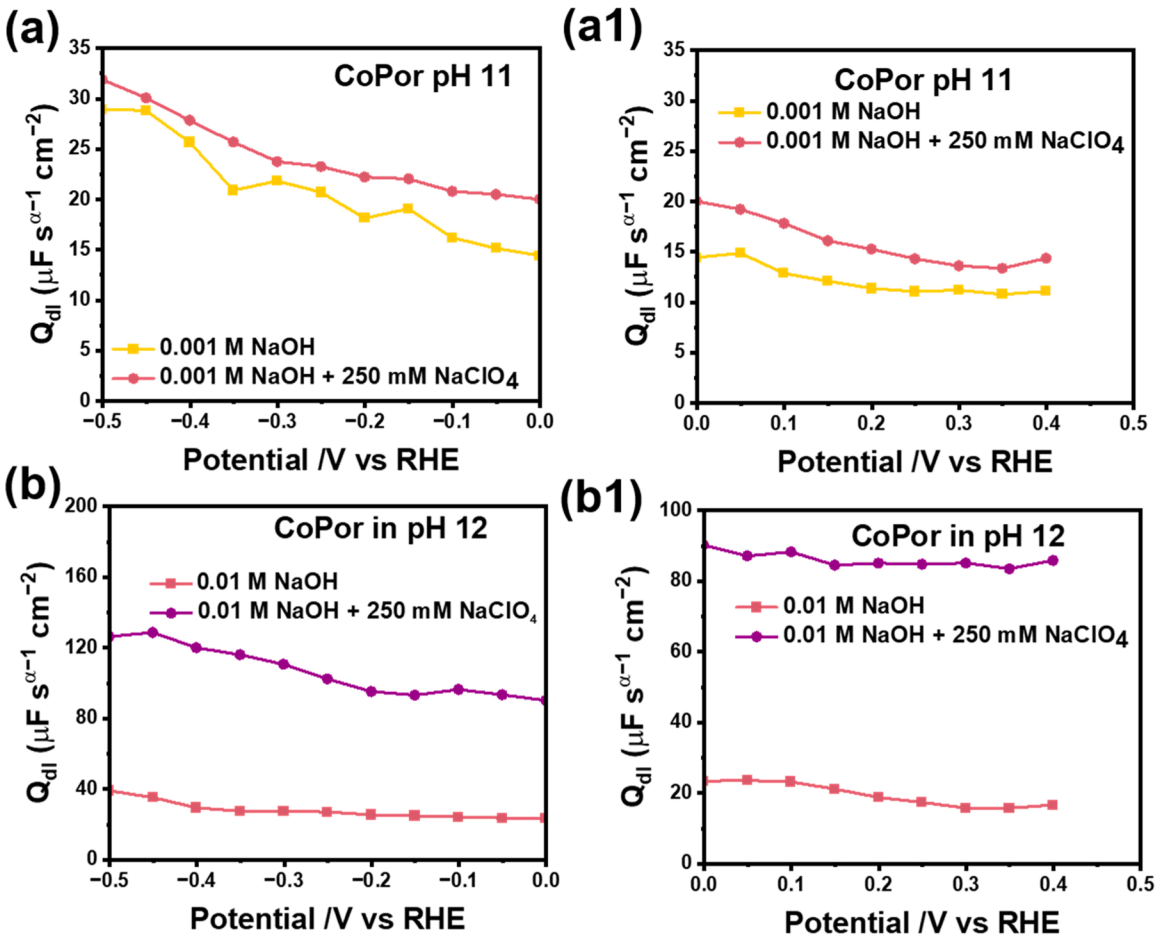

Fig. 7. Analysis of the influence of Na^+ concentration on Q_{dl} in pH 11 (a & a1) and pH 12 (b & b1) in the faradaic (a & b) and non-faradaic potential windows (a1 & b1).

advanced modeling and computational investigations, the remaining questions can be resolved. In the long run, we anticipate that gaining insights into how AMs^+ impact the very fundamental HER will enlighten and augment our understanding of more intricate catalytic systems and complex (electro)chemical reactions. In addition, it is crucial to highlight that the demonstrated electrochemical trends are apparent phenomena, mostly based on the bulk pH and bulk ionic strengths. However, it is critical to examine how the activity coefficient, interfacial pH and local cation concentration change in comparison with the bulk conditions and ultimately influence the HER activities.

5. Conclusion

As an alternative to scarce and expensive PGMs, CoPor and CoPc-based electrocatalysts were used to decipher the electrolytic effect of alkaline media on the HER activity. It was observed that the HER activity increases with increasing pH from 11 to 14. Also, a decrease in the Tafel slope indicates an improvement in the kinetics at pH 14, specifying the Volmer reaction as an RDS. When the nature of the present AMs^+ was analyzed, both CoPor and CoPc apparently followed the order of KOH>NaOH>LiOH. Interestingly, the Li^+ mostly showed the promoting effects on the HER throughout the pH range until pH 14, where a so-called saturation was achieved for CoPor. On the other hand, Na^+ and K^+ initially improved the HER activity of both electrocatalysts and then, after passing through a saturation level at pH 13, eventually inhibited the HER activity at pH 14 by demonstrating negative reaction orders. Moreover, as the RDE rotation rate increases, the HER activity presumably tends to drop. The estimation of double-layer capacitance using EIS indicated that enhanced concentration of AMs^+ at the reaction interface as the bulk pH or the concentration of the electrolyte increases, and indicates a direct correlation between HER activity and interfacial capacitance or local cation concentration. The presented research highlights the significance and complicated nature of the electrode/electrolyte interface during HER on the molecular electrocatalysts that would provide a basic understanding of the optimization of PGM-free electrocatalysis.

CRediT authorship contribution statement

Mohsin Muhyuddin: Writing – review & editing, Writing – original draft, Methodology, Investigation, Formal analysis, Data curation, Conceptualization. **Nicolò Pianta:** Writing – review & editing, Supervision, Formal analysis. **Jamie A Trindell:** Writing – review & editing, Methodology, Formal analysis. **Riccardo Ruffo:** Writing – review & editing, Supervision, Formal analysis. **Carlo Santoro:** Writing – review & editing, Supervision, Funding acquisition, Formal analysis. **Marc TM Koper:** Writing – review & editing, Supervision, Formal analysis, Conceptualization.

Declaration of competing interest

The authors declare that they have no known competing financial interests or personal relationships that could have appeared to influence the work reported in this paper.

Acknowledgments

C.S. and M.M. would like to acknowledge the NextGeneration EU from the Italian Ministry of Environment and Energy Security POR H2 AdP MMES/ENEA with involvement of CNR and RSE, PNRR - Mission 2, Component 2, Investment 3.5 "Ricerca e sviluppo sull'idrogeno" under the ENEA – UNIMIB agreement (Procedure 1.1.3 PNRR POR H_2). C.S. and M.M. would like to acknowledge the National recovery and resilience Plan (PNRR), Mission 2 "Green Revolution and Ecological Transition", Component 2 "Renewable Energy, Hydrogen, Network and Sustainable Mobility", Investment 3.5 "Hydrogen Research and Development", European Union – Next Generation EU – Italian Ministry of Environment and Energy Security (MASE), project AMBITION.

Supplementary materials

Supplementary material associated with this article can be found, in the online version, at doi:10.1016/j.electacta.2025.146684.

Data availability

Data will be made available on request.

References

[1] S. Trasatti, Work function, electronegativity, and electrochemical behaviour of metals: III. Electrolytic hydrogen evolution in acid solutions, Journal of Electroanalytical Chemistry and Interfacial Electrochemistry 39 (1) (Sep. 1972) 163–184, https://doi.org/10.1016/S0022-0728(72)80485-6.
[2] J.K. Nørskov, et al., Trends in the Exchange Current for Hydrogen Evolution, J. Electrochem. Soc. 152 (3) (Jan. 2005) J23, https://doi.org/10.1149/1.1856988.
[3] J.B. Mitchell, M. Shen, L. Twight, S.W. Boettcher, Hydrogen-evolution-reaction kinetics pH dependence: Is it covered? Chem Catalysis 2 (2) (Feb. 2022) 236–238, https://doi.org/10.1016/j.checat.2022.02.001.
[4] I.T. McCrum, M.T.M. Koper, The role of adsorbed hydroxide in hydrogen evolution reaction kinetics on modified platinum, Nat Energy 5 (11) (Nov. 2020) 891–899, https://doi.org/10.1038/s41560-020-00710-8.
[5] I. Ledezma-Yanez, W.D.Z. Wallace, P. Sebastián-Pascual, V. Climent, J.M. Feliu, M. T.M. Koper, Interfacial water reorganization as a pH-dependent descriptor of the hydrogen evolution rate on platinum electrodes, Nat Energy 2 (4) (Mar. 2017) 1–7, https://doi.org/10.1038/nenergy.2017.31.
[6] N. Mahmood, Y. Yao, J.-W. Zhang, L. Pan, X. Zhang, J.-J. Zou, Electrocatalysts for Hydrogen Evolution in Alkaline Electrolytes: Mechanisms, Challenges, and Prospective Solutions, Advanced Science 5 (2) (2018) 1700464, https://doi.org/10.1002/advs.201700464.
[7] R. Subbaraman, et al., Trends in activity for the water electrolyser reactions on 3d M(Ni,Co,Fe,Mn) hydr(oxy)oxide catalysts, Nature Mater 11 (6) (Jun. 2012) 550–557, https://doi.org/10.1038/nmat3313.
[8] J. Zhu, L. Hu, P. Zhao, L.Y.S. Lee, K.-Y. Wong, Recent Advances in Electrocatalytic Hydrogen Evolution Using Nanoparticles, Chem. Rev. 120 (2) (Jan. 2020) 851–918, https://doi.org/10.1021/acs.chemrev.9b00248.
[9] M. Muhyuddin, et al., Molybdenum disulfide as hydrogen evolution catalyst: From atomistic to materials structure and electrocatalytic performance, Journal of Energy Chemistry 87 (Dec. 2023) 256–285, https://doi.org/10.1016/j.jechem.2023.08.011.
[10] G.K. Gebremariam, A.Z. Jovanović, I.A. Pašti, The Effect of Electrolytes on the Kinetics of the Hydrogen Evolution Reaction, Hydrogen 4 (4) (Dec. 2023), https://doi.org/10.3390/hydrogen4040049. Art. no. 4.
[11] J. Li, et al., Multiple-interface relay catalysis: Enhancing alkaline hydrogen evolution through a combination of Volmer promoter and electrical-behavior regulation, Chemical Engineering Journal 397 (Oct. 2020) 125457, https://doi.org/10.1016/j.cej.2020.125457.
[12] Q. Dai, et al., Accelerated Water Dissociation Kinetics By Electron-Enriched Cobalt Sites for Efficient Alkaline Hydrogen Evolution, Advanced Functional Materials 32 (12) (2022) 2109556, https://doi.org/10.1002/adfm.202109556.
[13] L. Liu, Y. Liu, C. Liu, Enhancing the Understanding of Hydrogen Evolution and Oxidation Reactions on Pt(111) through Ab Initio Simulation of Electrode/Electrolyte Kinetics, J. Am. Chem. Soc. 142 (11) (Mar. 2020) 4985–4989, https://doi.org/10.1021/jacs.9b13694.
[14] L. Yuan, et al., Modulation of Volmer step for efficient alkaline water splitting implemented by titanium oxide promoting surface reconstruction of cobalt carbonate hydroxide, Nano Energy 82 (Apr. 2021) 105732, https://doi.org/10.1016/j.nanoen.2020.105732.
[15] S. Ringe, Cation effects on electrocatalytic reduction processes at the example of the hydrogen evolution reaction, Current Opinion in Electrochemistry 39 (Jun. 2023) 101268, https://doi.org/10.1016/j.coelec.2023.101268.
[16] B. Huang, et al., Cation- and pH-Dependent Hydrogen Evolution and Oxidation Reaction Kinetics, JACS Au 1 (10) (Oct. 2021) 1674–1687, https://doi.org/10.1021/jacsau.1c00281.
[17] S. Xue, et al., Influence of Alkali Metal Cations on the Hydrogen Evolution Reaction Activity of Pt, Ir, Au, and Ag Electrodes in Alkaline Electrolytes, ChemElectroChem 5 (17) (2018) 2326–2329, https://doi.org/10.1002/celc.201800690.
[18] B. Garlyyev, S. Xue, S. Watzele, D. Scieszka, A.S. Bandarenka, Influence of the Nature of the Alkali Metal Cations on the Electrical Double-Layer Capacitance of Model Pt(111) and Au(111) Electrodes, J. Phys. Chem. Lett. 9 (8) (Apr. 2018) 1927–1930, https://doi.org/10.1021/acs.jpclett.8b00610.
[19] J.T. Bender, et al., Understanding Cation Effects on the Hydrogen Evolution Reaction, ACS Energy Lett 8 (1) (Jan. 2023) 657–665, https://doi.org/10.1021/acsenergylett.2c02500.
[20] A. Goyal, M.T.M. Koper, The Interrelated Effect of Cations and Electrolyte pH on the Hydrogen Evolution Reaction on Gold Electrodes in Alkaline Media, Angewandte Chemie International Edition 60 (24) (2021) 13452–13462, https://doi.org/10.1002/anie.202102803.
[21] A. Goyal, M.T.M. Koper, Understanding the role of mass transport in tuning the hydrogen evolution kinetics on gold in alkaline media, The Journal of Chemical Physics 155 (13) (Oct. 2021) 134705, https://doi.org/10.1063/5.0064330.
[22] X. Chen, I.T. McCrum, K.A. Schwarz, M.J. Janik, M.T.M. Koper, Co-adsorption of Cations as the Cause of the Apparent pH Dependence of Hydrogen Adsorption on a Stepped Platinum Single-Crystal Electrode, Angewandte Chemie International Edition 56 (47) (2017) 15025–15029, https://doi.org/10.1002/anie.201709455.
[23] A.H. Shah, et al., The role of alkali metal cations and platinum-surface hydroxyl in the alkaline hydrogen evolution reaction, Nat Catal 5 (10) (Oct. 2022) 923–933, https://doi.org/10.1038/s41929-022-00851-x.
[24] M.C.O. Monteiro, A. Goyal, P. Moerland, M.T.M. Koper, Understanding Cation Trends for Hydrogen Evolution on Platinum and Gold Electrodes in Alkaline Media, ACS Catal 11 (23) (Dec. 2021) 14328–14335, https://doi.org/10.1021/acscatal.1c04268.
[25] D.J. Weber, M. Janssen, M. Oezaslan, Effect of Monovalent Cations on the HOR/HER Activity for Pt in Alkaline Environment, J. Electrochem. Soc. 166 (2) (Jan. 2019) F66, https://doi.org/10.1149/2.0301902jes.
[26] A. Goyal, S. Louisia, P. Moerland, M.T.M. Koper, Cooperative Effect of Cations and Catalyst Structure in Tuning Alkaline Hydrogen Evolution on Pt Electrodes, J. Am. Chem. Soc. 146 (11) (Mar. 2024) 7305–7312, https://doi.org/10.1021/jacs.3c11866.
[27] Y.-S. Hsu, S.T. Rathnayake, M.M. Waegele, Cation effects in hydrogen evolution and CO2-to-CO conversion: A critical perspective, The Journal of Chemical Physics 160 (16) (Apr. 2024) 160901, https://doi.org/10.1063/5.0201751.
[28] Z. Ma, et al., Recent advances of single-atom electrocatalysts for hydrogen evolution reaction, J. Phys. Mater. 4 (4) (Jun. 2021) 042002, https://doi.org/10.1088/2515-7639/ac01ac.
[29] B. Ren, J. Cao, H. Zhang, C. Han, W. Xu, Recent progress in the development of single-atom electrocatalysts for highly efficient hydrogen evolution reactions, Materials Chemistry Frontiers 7 (16) (2023) 3209–3231, https://doi.org/10.1039/D3QM00157A.
[30] A. Barrozo, M. Orio, Molecular Electrocatalysts for the Hydrogen Evolution Reaction: Input from Quantum Chemistry, ChemSusChem 12 (22) (2019) 4905–4915, https://doi.org/10.1002/cssc.201901828.
[31] S.A. Mirshokraee, et al., Ni-Phthalocyanine Derived Electrocatalysts for Oxygen Reduction Reaction and Hydrogen Evolution Reaction: Active Sites Formation and Electrocatalytic Activity, ACS Catal 14 (19) (Oct. 2024) 14524–14538, https://doi.org/10.1021/acscatal.4c03814.
[32] J. Wang, W. Cui, Q. Liu, Z. Xing, A.M. Asiri, X. Sun, Recent Progress in Cobalt-Based Heterogeneous Catalysts for Electrochemical Water Splitting, Advanced Materials 28 (2) (2016) 215–230, https://doi.org/10.1002/adma.201502696.
[33] R. Sun, et al., Recent advances in cobalt-based catalysts for efficient electrochemical hydrogen evolution: a review, Dalton Trans 51 (40) (Oct. 2022) 15205–15226, https://doi.org/10.1039/D2DT02189G.
[34] Y. Wang, et al., Electrolyte Effect on Electrocatalytic Hydrogen Evolution Performance of One-Dimensional Cobalt–Dithiolene Metal–Organic Frameworks: A Theoretical Perspective, ACS Appl. Energy Mater. 1 (4) (Apr. 2018) 1688–1694, https://doi.org/10.1021/acsaem.8b00174.
[35] H. Li, et al., Multiscale engineering of molecular electrocatalysts for the rapid hydrogen evolution reaction, Nano Res (May 2024), https://doi.org/10.1007/s12274-024-6660-z.
[36] L. Chen, et al., Cobalt phthalocyanine as an efficient catalyst for hydrogen evolution reaction, International Journal of Hydrogen Energy 46 (37) (May 2021) 19338–19346, https://doi.org/10.1016/j.ijhydene.2021.03.075.
[37] K.P. Cp, S. Aralekallu, V.A. Sajjan, M. Palanna, S. Kumar, L.K. Sannegowda, Non-precious cobalt phthalocyanine-embedded iron ore electrocatalysts for hydrogen evolution reactions, Sustainable Energy Fuels 5 (5) (Mar. 2021) 1448–1457, https://doi.org/10.1039/D0SE01829E.
[38] N. Kousar, Giddaerappa, L.K. Sannegowda, Hybrid cobalt phthalocyanine polymer as a potential electrocatalyst for hydrogen evolution reaction, International Journal of Hydrogen Energy 50 (Jan. 2024) 37–47, https://doi.org/10.1016/j.ijhydene.2023.06.296.
[39] Y. Dou, et al., Efficient hydrogen generation of a cobalt porphyrin-bridged covalent triazine polymer, Journal of Colloid and Interface Science 644 (Aug. 2023) 256–263, https://doi.org/10.1016/j.jcis.2023.04.082.
[40] H. Sheng, et al., Strong synergy between gold nanoparticles and cobalt porphyrin induces highly efficient photocatalytic hydrogen evolution, Nat Commun 14 (1) (Mar. 2023) 1528, https://doi.org/10.1038/s41467-023-37271-9.

[41] Y. Wu, J.M. Veleta, D. Tang, A.D. Price, C.E. Botez, D. Villagrán, Efficient electrocatalytic hydrogen gas evolution by a cobalt–porphyrin-based crystalline polymer, Dalton Trans 47 (26) (Jul. 2018) 8801–8806, https://doi.org/10.1039/C8DT00302E.
[42] B.B. Beyene, S.B. Mane, C.-H. Hung, Electrochemical Hydrogen Evolution by Cobalt (II) Porphyrins: Effects of Ligand Modification on Catalytic Activity, Efficiency and Overpotential, J. Electrochem. Soc. 165 (9) (Jun. 2018) H481, https://doi.org/10.1149/2.0481809jes.
[43] C.J. Kaminsky, S. Weng, J. Wright, Y. Surendranath, Adsorbed cobalt porphyrins act like metal surfaces in electrocatalysis, Nat Catal 5 (5) (May 2022) 430–442, https://doi.org/10.1038/s41929-022-00791-6.
[44] Y. Liu, C.C.L. McCrory, Modulating the mechanism of electrocatalytic CO2 reduction by cobalt phthalocyanine through polymer coordination and encapsulation, Nat Commun 10 (1) (Apr. 2019) 1683, https://doi.org/10.1038/s41467-019-09626-8.
[45] S. Lin, et al., Covalent organic frameworks comprising cobalt porphyrins for catalytic CO2 reduction in water, Science 349 (6253) (Sep. 2015) 1208–1213, https://doi.org/10.1126/science.aac8343.
[46] Z.-S. Wu, et al., High-Performance Electrocatalysts for Oxygen Reduction Derived from Cobalt Porphyrin-Based Conjugated Mesoporous Polymers, Advanced Materials 26 (9) (2014) 1450–1455, https://doi.org/10.1002/adma.201304147.
[47] W. Fan, et al., Rational design of heterogenized molecular phthalocyanine hybrid single-atom electrocatalyst towards two-electron oxygen reduction, Nat Commun 14 (1) (Mar. 2023) 1426, https://doi.org/10.1038/s41467-023-37066-y.
[48] B. Liu, C. Brückner, Y. Lei, Y. Cheng, C. Santoro, B. Li, Cobalt porphyrin-based material as methanol tolerant cathode in single chamber microbial fuel cells (SCMFCs), Journal of Power Sources 257 (Jul. 2014) 246–253, https://doi.org/10.1016/j.jpowsour.2014.01.117.
[49] H.C. Honig, et al., Morphological and structural design through hard-templating of PGM-free electrocatalysts for AEMFC applications, Nanoscale 16 (23) (2024) 11174–11186, https://doi.org/10.1039/D4NR01779J.
[50] M. Muhyuddin, et al., Enhancing Electrocatalysis: Engineering the Fe–Nx–C Electrocatalyst for Oxygen Reduction Reaction Using Fe-Functionalized Silica Hard Templates, ACS Appl. Energy Mater. (Dec. 2024), https://doi.org/10.1021/acsaem.4c01215.
[51] M.C.O. Monteiro, X. Liu, B.J.L. Hagedoorn, D.D. Snabilié, M.T.M. Koper, Interfacial pH Measurements Using a Rotating Ring-Disc Electrode with a Voltammetric pH Sensor, ChemElectroChem 9 (1) (2022) e202101223, https://doi.org/10.1002/celc.202101223.
[52] X. Liu, M.C.O. Monteiro, M.T.M. Koper, Interfacial pH measurements during CO2 reduction on gold using a rotating ring-disk electrode, Phys. Chem. Chem. Phys. 25 (4) (Jan. 2023) 2897–2906, https://doi.org/10.1039/D2CP05515E.
[53] A. Goyal, G. Marcandalli, V.A. Mints, M.T.M. Koper, Competition between CO2 Reduction and Hydrogen Evolution on a Gold Electrode under Well-Defined Mass Transport Conditions, J. Am. Chem. Soc. 142 (9) (Mar. 2020) 4154–4161, https://doi.org/10.1021/jacs.9b10061.
[54] J. Resasco, Y. Lum, E. Clark, J.Z. Zeledon, A.T. Bell, Effects of Anion Identity and Concentration on Electrochemical Reduction of CO2, ChemElectroChem 5 (7) (2018) 1064–1072, https://doi.org/10.1002/celc.201701316.
[55] O. Jung, M.N. Jackson, R.P. Bisbey, N.E. Kogan, Y. Surendranath, Innocent buffers reveal the intrinsic pH- and coverage-dependent kinetics of the hydrogen evolution reaction on noble metals, Joule 6 (2) (Feb. 2022) 476–493, https://doi.org/10.1016/j.joule.2022.01.007.
[56] L. Rebollar, et al., Beyond Adsorption" Descriptors in Hydrogen Electrocatalysis, ACS Catal 10 (24) (Dec. 2020) 14747–14762, https://doi.org/10.1021/acscatal.0c03801.
[57] S. Tanaka, H. Tajiri, O. Sakata, N. Hoshi, M. Nakamura, Interfacial Structure of Pt (110) Electrode during Hydrogen Evolution Reaction in Alkaline Solutions, J. Phys. Chem. Lett. 13 (36) (Sep. 2022) 8403–8408, https://doi.org/10.1021/acs.jpclett.2c01575.
[58] S. Xue, B. Garlyyev, A. Auer, J. Kunze-Liebhäuser, A.S. Bandarenka, How the Nature of the Alkali Metal Cations Influences the Double-Layer Capacitance of Cu, Au, and Pt Single-Crystal Electrodes, J. Phys. Chem. C 124 (23) (Jun. 2020) 12442–12447, https://doi.org/10.1021/acs.jpcc.0c01715.
[59] L. Shen, A. Goyal, X. Chen, M.T.M. Koper, Cation Effects on Hydrogen Oxidation Reaction on Pt Single-Crystal Electrodes in Alkaline Media, J. Phys. Chem. Lett. 15 (10) (Mar. 2024) 2911–2915, https://doi.org/10.1021/acs.jpclett.4c00292.
[60] R. Punathil Meethal, R. Saibi, R. Srinivasan, Hydrogen evolution reaction on polycrystalline Au inverted rotating disc electrode in HClO4 and NaOH solutions, International Journal of Hydrogen Energy 47 (31) (Apr. 2022) 14304–14318, https://doi.org/10.1016/j.ijhydene.2022.02.177.
[61] S.A. Watzele, R.M. Kluge, A. Maljusch, P. Borowski, A.S. Bandarenka, Impedance Response Analysis of Anion Exchange Membrane Electrolyzers for Determination of the Electrochemically Active Catalyst Surface Area, Chemistry–Methods 4 (3) (2024) e202300035, https://doi.org/10.1002/cmtd.202300035.
[62] S. Watzele, J. Fichtner, B. Garlyyev, J.N. Schwämmlein, A.S. Bandarenka, On the Dominating Mechanism of the Hydrogen Evolution Reaction at Polycrystalline Pt Electrodes in Acidic Media, ACS Catal 8 (10) (Oct. 2018) 9456–9462, https://doi.org/10.1021/acscatal.8b03365.
[63] Allen J. Bard, Larry R. Faulkner, Electrochemical Methods: Fundamentals and Applications, in: Russian Journal of Electrochemistry, 2nd ed., 38, Wiley, New York, 2001, pp. 1364–1365, https://doi.org/10.1023/A:1021637209564. Dec. 2002.